

# A multiplexed control architecture for superconducting qubits with row-column addressing

Peng Zhao<sup>1,2, \*</sup>

<sup>1</sup>Tongling, Anhui 244000, China

<sup>2</sup>Beijing Academy of Quantum Information Sciences, Beijing 100193, China

(Dated: March 21, 2024)

In state-of-the-art superconducting quantum processors, each qubit is controlled by at least one control line that delivers control pulses generated at room temperature to qubits operating at millikelvin temperatures. While this strategy has been successfully applied to control hundreds of qubits, it is unlikely to be scalable to control thousands of qubits, let alone millions or even billions of qubits needed in fault-tolerance quantum computing. The primary obstacle lies in the wiring challenge, wherein the number of accommodated control lines is limited by factors, such as the cooling power, physical space of the cryogenic system, the control footprint area at the qubit chip level, and so on. Here, we introduce a multiplexed control architecture for superconducting qubits with two types of shared control lines, row and column lines, providing an efficient approach for parallel controlling  $N$  qubits with  $O(\sqrt{N})$  control lines. With the combination of the two-type shared lines, unique pairs of control pulses are delivered to qubits at each row-column intersection, enabling parallel qubit addressing. Of particular concern here is that, unlike traditional gate schemes, both single- and two-qubit gates are implemented with pairs of control pulses. Considering the inherent parallelism and the control limitations, the integration of the architecture into quantum computing systems should be tailored as much as possible to the specific properties of the quantum circuits to be executed. As such, the architecture could be scalable for executing structured quantum circuits, such as quantum error correction circuits.

## I. INTRODUCTION

To perform quantum computing with noisy qubits for solving valuable problems that are intractable for classical computing, quantum error correction (QEC) is widely recognized as the ultimate solution [1, 2]. To date, among the various candidate quantum systems for realizing QEC, superconducting qubits have been demonstrated as a leading one [3–7]. In a superconducting quantum processor with tens of qubits, a recent experiment has shown that QEC begins to suppress logical errors with increasing system sizes [7]. Nevertheless, to fully utilize the power of QEC, such as surface code [2, 8], in quantum computing, it is generally believed that high-fidelity control over millions or even billions of qubits is required [8, 9].

In state-of-the-art superconducting quantum processors, shown in Fig. 1(a), each qubit is controlled by at least one control line, which delivers dedicated control pulses generated at room temperature to qubits operating at millikelvin temperatures [10–12]. For controlling a  $N$ -qubit system, the number of control lines (input-output connections, IOs) at room temperature ( $P_{RT}$ ) and in the dilution refrigerator ( $P_{cryo}$ ) is dictated by the IO terminals of the qubit chip ( $P_{chip}$ ), scaling linearly with the qubit number  $N$ , see Fig. 1(b), resulting in  $P_{RT} = P_{cryo} = P_{chip} \sim O(N)$  [13]. This independent control strategy offers great flexibility in controlling qubits [12] and is applied to achieve low gate errors across small-scale systems comprising tens or hundreds of qubits. However, the scalability of this approach to larger systems is hindered by challenges such as heating loads from the control lines [11], non-negligible feature sizes of cables or IO terminals, and the requirement of at least one digital-to-analog converter (DAC)

per line for qubit control [12]. These limitations highlight the wiring challenge associated with scaling up quantum processors [13–16], where the number of manageable control lines is limited by factors including cooling power, geometric constraints of the cryogenic system, control footprint area at the qubit chip level, and the overhead of classical electronics. To facilitate a more intuitive understanding of this challenge, consider that to control a superconducting quantum processor with a few thousand qubits, the number of required control lines or IOs would be comparable to that needed to manage one billion transistors in state-of-the-art classical processors [14]. In this sense, the wiring challenges need to be addressed before a large-scale superconducting quantum processor becomes feasible.

To alleviate the wiring challenge in superconducting quantum systems, various strategies which aim to reduce the control lines running from room temperature to cryogenic temperature, i.e., achieving  $P_{RT} < P_{cryo}$ , have been explored [17–25]. One of the most widely studied approaches is the implementation of cryogenic control electronics operated at 4 K [19–24] or 10 mK [23–25], but implementing successful qubit control at scale while achieving ultra-low-power dissipation remains challenging. Additionally, on-chip control electronics have also been explored to reduce the chip IO terminals [19, 26]. However, as the control footprint area at the chip level is limited by qubit size, besides the heating dissipation and the newly added noises, the on-chip integration can increase the complexity of wire routing, especially when scaling up. Therefore, a common view is that only taking these strategies alone is unlikely to address the wiring challenge [14].

Besides the above top-down approaches, one alternative that has emerged from taking a bottom-up perspective involves leveraging multiplexed qubit control with shared lines to reduce line overhead. This perspective has been extensively explored for semiconductor spin qubits [14, 27–29] and super-

\*Electronic address: [shangniguo@sina.com](mailto:shangniguo@sina.com)

conducting quantum annealing processors [30, 31]. For superconducting qubits, the most successful demonstration is the frequency-multiplexed qubit readout [32–34], where a single feedline is shared by several readout circuitries, enabling simultaneous readout of several qubits. However, exploring the multiplexing for qubit control is still in its infancy [35–38]. Unlike the independent qubit control, the multiplexed control will degrade the control flexibility. Thus, to realize quantum computing, generally, new control overhead or hardware components shall be introduced [37, 38]. Most importantly, further demonstrations of these new features that are compatible with high-fidelity qubit control are required.

In this work, we propose a multiplexed control architecture for superconducting qubits with row-column addressing, offering the potential for parallel control of  $N$  qubits with  $O(\sqrt{N})$  control lines. By incorporating both row and column shared control lines, unique pairs of control pulses are delivered to qubits or couplers at each row-column intersection, allowing parallel single- or two-qubit gate operations in qubit lattices. Accordingly, we present various single- and two-qubit schemes that are both compatible with the row-column addressing and the existing superconducting qubit technologies (with no new hardware components). We further show that while the control flexibility is compromised, the inherent parallelism of the architecture makes it well-suited for executing structured quantum circuits, which comprise layers of parallel single- or two-qubit gates across qubit lattices, such as QEC circuits.

We note that very recently, a similar scheme for selectively addressing qubits has also been studied in semiconductor spin qubits [39–41] by using two microwave drives and has been proposed to enable parallel single-qubit gates [39].

The paper is organized as follows. In Sec. II, we first provide an overview of the multiplexed control architecture. Then, in QEC with surface code, we illustrate that the integration of the architecture into quantum computing systems should be tailored to specific quantum circuits. In Sec. III, we give detailed descriptions of the single- and two-qubit gate schemes that support row-column addressing. In Sec. IV, we discuss the challenges to be faced when scaling up. Finally, in Sec. V, we provide a summary of our study.

## II. THE MULTIPLEXED CONTROL ARCHITECTURE WITH ROW-COLUMN ADDRESSING

For controlling two-dimensional (2D) square qubit lattices, Figure 1(c) schematically shows the multiplexed control architecture, which comprises two types of shared control lines, row lines and column lines. The qubits are located on the intersections of the two-type lines, with qubit connected (coupled) to a distinct pair of control lines, enabling spatial qubit addressing. By simultaneously applying appropriate pulses to the shared control lines, each qubit can be driven by a unique pair of control pulses through the associated row and column lines, as depicted in Fig. 1(c). As we will discuss in the next section, when the pair of control pulses satisfies certain conditions, single- or two-qubit gate operations can be realized.

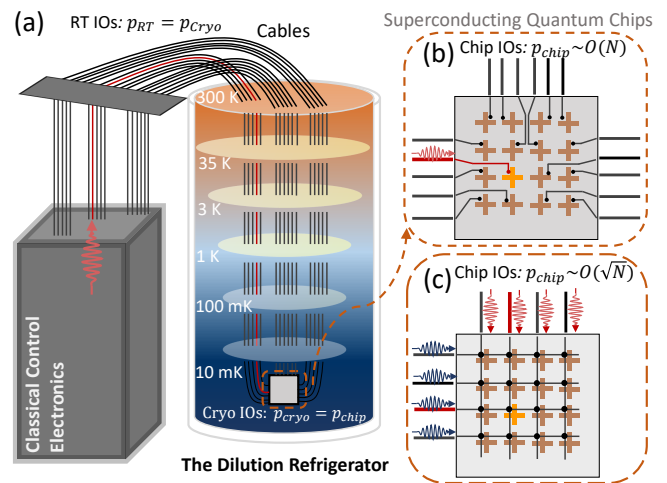


FIG. 1: Schematic (not to scale) of a typical superconducting quantum computing system. (a) Qubits at millikelvin temperatures are controlled using control pulses generated by classical electronics at room temperature and delivered through cables. The number of control lines (input-output connections, IOs) at room temperature  $P_{RT}$  and the number of cables in the dilution refrigerator  $P_{cryo}$  are determined by the number of input-output (IO) terminals of the chip  $P_{chip}$ , leading to  $P_{RT} = P_{cryo} = P_{chip}$ . (b) With the independent control,  $P_{chip} \sim O(N)$ , where  $N$  is the qubit number. This strategy offers maximum flexibility in qubit control, enabling individual addressing without affecting other qubits (see the qubit highlighted in light orange). (c) In the multiplexed control architecture, applying appropriate pulses to control lines simultaneously allows unique pairs of control pulses to be delivered to qubits at the intersection of row lines and column lines, enabling parallel qubit addressing. Hence, the IO terminals  $P_{chip}$  scales with  $\sqrt{N}$ . Here, each qubit (see the qubit highlighted in light orange) or any subgroup of qubits cannot be individually addressed without affecting all other idle qubits.

Thus, this control strategy can be well suited for performing parallel addressing, allowing simultaneous single- or two-qubit gates across the qubit lattice.

However, due to the shared nature of the control lines among qubits, selective addressing of individual qubits or specific subgroups (i.e., for implementing non-structured quantum circuits) without impacting all other idle (inactive) qubits is challenging [42]. For example, as shown in Fig. 1(c), when one considers addressing the qubit highlighted in light orange, two pulses are delivered to the associated row and column lines. Consequently, idle qubits coupled to the same row or column control lines can be driven by one of the two shared pulses, causing idling qubit errors. Similarly, one can envision a scenario in which fine-tuned gate pulses are simultaneously applied to all the shared lines. This allows gate operations on select qubits to be executed successfully. However, the non-selective (inactive) qubits are also driven by pairs of pulses, potentially leading to idle gate errors. Note that as each qubit is controlled by a unique pair of gate pulses, this allows for tailored design of pulses to implement distinct gates on individual qubits. For instance, target gates can be applied to the active qubits while identity operations can be performed on

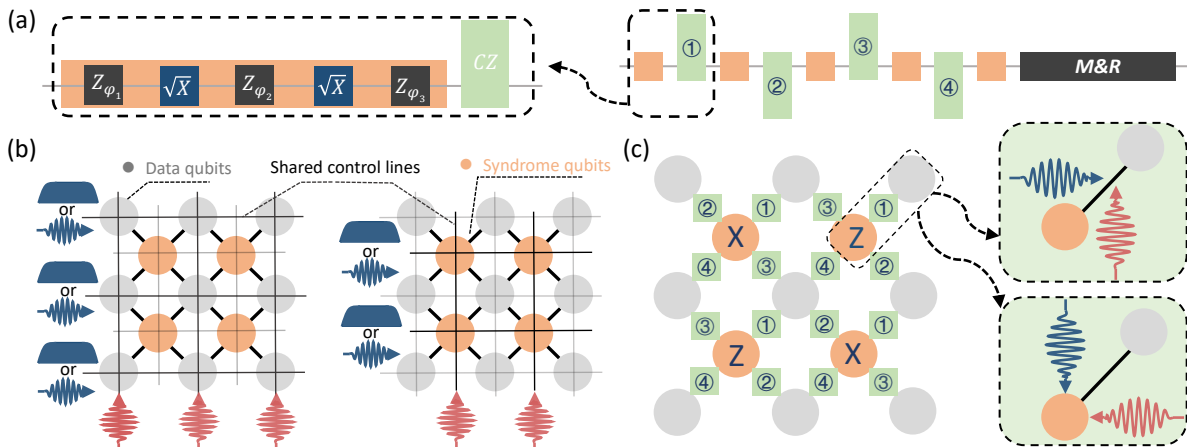


FIG. 2: Multiplexed qubit control for QEC with surface code. (a) A typical stabilizer measurement circuit in surface code using CZ gates, with the single-qubit gate decomposed into two  $\sqrt{X}$  gates and three Z gates. During the QEC cycle, interleaved single- and two-qubit gates are implemented and at the end of the cycle, syndrome qubits are measured first and then reset while data qubits are idle. (b) Two sets of shared control lines are employed for independent addressing of data qubits and syndrome qubits. This setup ensures compatibility between the multiplexed control architecture and QEC circuits, which involve dynamical decoupling sequences to reduce qubit idling errors and two-qubit gates with one-qubit driving. The shared control lines can deliver microwave or flux pulses for qubit control. (c) In QEC with surface code, the sequence of two-qubit gates depends on the type of syndrome qubits (Z-type or X-type), resulting in four different patterns for the sequence of two-qubit gates in the QEC cycle. Hence, for QEC based on two-qubit gates with driven couplers, besides shared lines for qubit addressing, an extra four sets of shared lines are required for selectively choosing gate patterns.

the idle qubits. However, this approach generally results in the introduction of additional overheads in gate calibration.

In comparison to the independent control, there exist two features in controlling qubits. The first feature involves the trade-off between multiplexed control and control flexibility. While multiplexed control can reduce control flexibility, it effectively addresses wiring challenges by enabling parallel control of  $N$  qubits with  $O(\sqrt{N})$  lines. The second feature pertains to the requirement for both single- and two-qubit gates to be executed using a pair of control pulses, thereby supporting row-column addressing. Consequently, two key issues emerge within this architecture: the impact of reduced control flexibility on the utility of multiplexed control in quantum computing, and the validation of gate operations that support row-column addressing. In the subsequent discussion, we aim to first tackle the former one. We will start with a discussion of being agnostic to the physical details of qubits and gate schemes, which will be elaborated in the next section.

Despite the compromise in control flexibility, the inherent parallelism of the multiplexed control could allow for executing structured quantum circuits, which consist of layers of parallel single- and two-qubit gates across qubit systems (note that by using the isomorphous waveform technique introduced in Ref. [43], an arbitrary quantum circuit comprising modular single- and two-qubit gates can be compiled into structured quantum circuits). Nevertheless, for practicality and utility, the multiplexed control should be tailored to be compatible with the specific properties of the structured circuits.

Here, we consider the realization of a QEC circuit with the multiplexed control scheme. Figure 2(a) shows the typical quantum circuit for stabilizer measurements in surface

code using CZ gates [7], where the single-qubit gate (including the identity gate) is decomposed into two  $\sqrt{X}$  gates and three Z gates [44] (the rationale behind this decomposition will be addressed in the subsequent section). Throughout the QEC cycle, interleaved single- and two-qubit gates are implemented and at the end of the cycle, syndrome qubits are measured first and then reset while data qubits are idle. To ensure compatibility with the QEC circuit, Figure 2(b) presents the multiplexed control architecture comprising two sets of shared row-column lines for independently addressing data qubits and syndrome qubits. This tailored setting is adopted for two reasons: (i) during the syndrome measurement and reset, dynamical decoupling comprising a sequence of single-qubit gates is generally applied to data qubits for suppressing idling errors (currently the predominant error source) [7]; (ii) in certain two-qubit gate schemes, only one of the qubits, such as the syndrome qubit shown in Fig. 2(c), is driven by control pulses [45, 46].

Additionally, as depicted in Fig. 2(c), specific two-qubit gate schemes involve applying control pulses solely to couplers [47–50]. Meanwhile, in stabilizer measurement circuits of the surface code, the order of two-qubit gates depends on the syndromes being measured, either Z or X. This gives rise to four different patterns for the sequence of two-qubit gates in QEC cycles [1, 2], as shown in Fig. 2(c). Therefore, to minimize any aforementioned idle errors and calibration overhead, besides the shared lines for qubit addressing, an extra four sets of shared lines can be introduced for selectively choosing the gate pattern and addressing couplers.

Before leaving this section, note that although we only focus on QEC circuits, there is potential for adapting the multi-

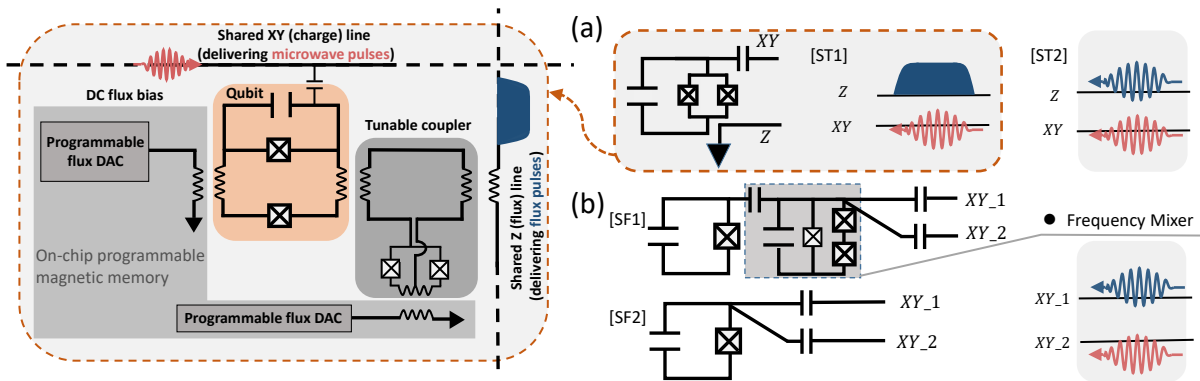


FIG. 3: Schematic illustration of single-qubit gate schemes with two control pulses. (a) Single-qubit gates applied to frequency-tunable transmon qubits. During gate operations, a flux pulse and a microwave pulse are simultaneously delivered to the qubit through the Z line and the XY line, respectively. Static dc flux biases are needed for biasing the qubits at their idle points and are realized by using an on-chip programmable magnetic memory such as  $\Phi$ -DAC. (ST1) illustrates the gate scheme based on tuning the qubit on-resonance with the microwave drive pulse using a baseband flux pulse. Individual tuning of the coupling between the Z line and the qubit is enabled by a tunable rf-SQUID coupler biased by a  $\Phi$ -DAC. (ST2) shows the gate scheme that utilizes the combination of parametric drive and microwave drive. Due to the nonlinear dependence of the qubit frequency on the flux bias, the parametric-driven qubit can have a series of sideband frequency components. When one of such sidebands is on-resonance with the microwave drive, qubit control can be achieved. (b) Single-qubit gates for fixed-frequency transmon qubits. During gates, a pair of microwave drive pulses are simultaneously delivered to the qubit through the two XY lines. (SF1) depicts the gate scheme using the three-wave mixing process mediated by a flux qubit. When the sum-frequency or difference-frequency of the two drives is on-resonance with the qubit, the qubit can be controlled by an effective on-resonance drive. (SF2) displays the gate scheme that uses one off-resonance microwave drive to control a qubit dressed by a second off-resonance drive.

plexed control scheme for logical operations as well. This is supported by the following three key observations. First, logical operations, such as those based on lattice surgery [51], in essence, involve different patterns of stabilizer measurements that are compatible with the multiplexed control. Second, a more tailored setting can be introduced for patterns of stabilizers that are incompatible with the above setting and the added line overhead can scale with  $\sqrt{N}$ . Third, while selectively addressing specific qubit subgroups to accommodate stabilizer patterns for logical operations may cause qubit idling errors, such as phase errors due to off-resonance drives, this could be compensated in subsequent QEC cycles, albeit potentially leading to an increase in circuit depth.

### III. GATE OPERATIONS IN THE MULTIPLEXED CONTROL ARCHITECTURE

Here we turn to illustrate how single- and two-qubit gates are realized in the multiplexed control architecture. As shown in Figs. 1(c) and 2, gate operations, unlike that in the conventional independent control scheme, are implemented by applying simultaneous control pulses to all shared row and column lines. When focusing on one particular qubit or coupler within the lattice, single- and two-qubit gate operations are realized by applying a unique pair of control pulses to a qubit or a coupler. Within this context, we propose various gate schemes that are both compatible with the two-pulse configuration and the existing superconducting qubit technologies. For illustration purposes, we focus on the gates applied to transmon qubits [53], but in principle, it should also be feasible for other

superconducting qubits, such as fluxonium qubits [54].

#### A. Single-qubit gates

TABLE I: Single-qubit gate schemes with two control pulses. The schematic illustration of these schemes is shown in Fig. 3. Note that for frequency-tunable qubits, static dc flux biases (not listed here but shown in Fig. 3) are generally required to bias the qubits at their idle points.

Specific	Single-qubit addressing strategy
Tunable element	(ST1) Baseband flux bias + microwave drive [36, 37];
	(ST2) Flux modulation + microwave drive [35];
Fixed element	(SF1) Frequency mixer: e.g. three-wave mixing [55–58];
	(SF2) Two-tone microwave drive [59–63];

Table I summarizes four single-qubit gate schemes using two control pulses, which are also schematically illustrated in Fig. 3. These schemes can be grouped into two categories, depending on whether the qubit is tunable. In the following, we will delve into detailed explanations of each of the four gate schemes.

*Type-ST*: This category pertains to single-qubit gates designed for frequency-tunable qubits. During gate operations, a flux pulse and a microwave pulse are simultaneously delivered to the qubit through a shared Z line and a shared XY line, respectively, as shown in Fig. 3(a). Furthermore, for frequency-tunable qubits, static dc flux biases are generally

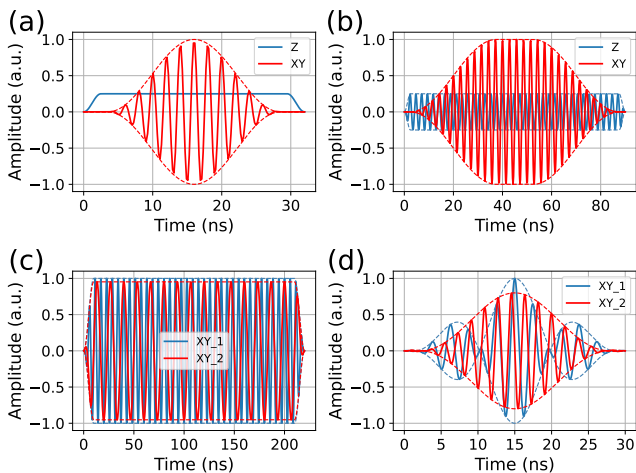


FIG. 4: The control pulses for single-qubit gate schemes schematically illustrated in Fig. 3 (also summarized in Table I). The dashed lines denote the pulse envelopes. (a) shows the pulses for the gate scheme (ST1), using a 25-ns cosine DRAG pulse and a flat-top baseband pulse with a cosine ramp of 2.5 ns. Here, a delay of 1 ns is inserted between the two pulses, giving rise to the total gate length of 32 ns. (b) shows the pulses for the gate scheme (ST2), using a flat-top parametric drive pulse with the ramp time of 2.5 ns and a flat-top microwave drive pulse with the ramp time of 35 ns. The total gate length is 90 ns. (c) shows the pulses for the gate scheme (SF1), using two 220-ns flat-top microwave drive pulses with the same ramp time of 10 ns. (d) shows the pulses for the gate scheme (SF2), using two 30-ns DRAG pulses. Note here that the DRAG coefficient is  $\alpha = 1$  for suppressing leakage and only the in-phase component of the cosine DRAG pulse is shown for clarity.

needed for biasing the qubits at their idle points. Following Ref. [30], this flux offset can in principle be introduced by using a  $\Phi$ -DAC, which functions as on-chip programmable magnetic memory and provides the required static bias. Moreover, the  $\Phi$ -DAC can be efficiently programmed and addressed by the addressing circuitry, which requires  $O(\sqrt[3]{N})$  control lines for  $N$  frequency-tunable qubits [31].

(ST1) This control scheme involves a microwave drive pulse and a baseband flux pulse. Similar to Refs. [36, 37], single-qubit gates, such as  $\sqrt{X}$  gates, are realized by individually tuning qubits on resonance with the shared microwave drive. Unlike previous works using an always-on microwave drive [37], here a microwave drive pulse is used to prevent any negative effects on other qubit operations, such as qubit readout, qubit reset, and two-qubit gates. Thus the derivative removal by adiabatic gate (DRAG) can be employed for realizing single-qubit gates [64]. Figure 4(a) shows the typical two-pulse configuration, which consists of a raised cosine flat-top flux pulse for tuning the qubit frequency from the idle point to the working point and a cosine DRAG pulse for XY control [65]. As qubit idling frequencies should be different from qubits to qubits, the amplitude of the flux pulse applied to each qubit should be individually fine-tuned to resonate with the shared microwave drive. Given that the flux pulse is applied globally to qubits through the shared Z lines,

individual tuning is required and can be achieved by realizing tunable coupling between qubits and the shared Z lines. Following Ref. [30], Figure 3(a) shows the tunable rf-SQUID coupler [66–68], which itself is controlled by a  $\Phi$ -DAC, for individually tuning the amplitudes of flux pulses felt by qubits.

(ST2) This scheme entails a parametric drive pulse through the Z line and a microwave drive pulse through the XY line. As illustrated in Refs.[35, 46, 69], modulating the qubit frequency with a parametric drive can induce a series of sidebands due to the nonlinear dependence of the qubit frequency on the flux bias. When one of these sidebands is on-resonance with the microwave drive, it enables coherent qubit control [35]. Figure 4(b) shows this pulse configuration, where a flat-top parametric drive pulse with cosine-shape ramps modulates the qubit frequency and a raised cosine flat-top microwave drive pulse facilitates XY control. Note that similar schemes have also been studied recently in semiconductor spin qubits [39–41].

*Type-SF:* This category pertains to single-qubit gates intended for fixed-frequency qubits. During single-qubit gates, a pair of microwave drive pulses are simultaneously delivered to the qubit through the two XY lines, as shown in Fig. 3(b).

(SF1) Leveraging an on-chip ‘three-wave mixer’ [55–58], the two microwave drives are converted to an effective qubit drive. When the sum-frequency or difference-frequency of the two drives is on-resonance with the qubit, coherent control of the qubit can be achieved with the effective drive. Figure 3(b) schematically illustrates such an on-chip mixer based on flux qubit [57, 58], which is capacitively coupled to the transmon qubit and is driven by the two microwave drives. Here, for example, we consider that the difference frequency of pulses equals the qubit frequency. Accordingly, Figure 4(c) shows the typical used raised cosine flat-top pulses.

(SF2) In this scenario, single-qubit gates are realized by applying two off-resonance microwave drives to the qubit [59–63], as shown in Fig. 3(b). Such scheme can be understood as follows: one of the two off-resonance drives is used to dress the (bare) qubit and shift the qubit frequency through the ac-Stark effect, while the second one is applied for controlling such a microwave-dressed qubit [70–72]. Moreover, this two-tone drive scheme can be combined with the DRAG scheme to suppress leakage errors during gate operations. Figure 4(d) depicts the typical used cosine DRAG pulses in this context.

For each of the schemes depicted in Fig. 3 (also summarized in Table I), Figure 5 presents the numerical verification of their feasibility for performing single-qubit gates, e.g.,  $\sqrt{X}$  gates or  $X$  gates, according to the control pulses shown in Fig. 4. Here, the upper panel shows the population ( $P_0$ ) in state  $|0\rangle$  at the end of the applied pulses with the qubit prepared in its ground state. The dashed grey line denotes the feasible regions of the control parameters for realizing  $\sqrt{X}$  gates while the red star is for  $X$  gates. Furthermore, the bottom panel shows the leakage  $L_1$  [73]. These numerical findings indicate that low-leakage, high-fidelity single-qubit  $X$  rotations can be achieved with the proposed schemes.

As shown in Fig. 2(a), to achieve universal single-qubit control, we consider compiling arbitrary single-qubit gates into two  $\sqrt{X}$  gates and three physical (or virtual)  $Z$  gates [44].

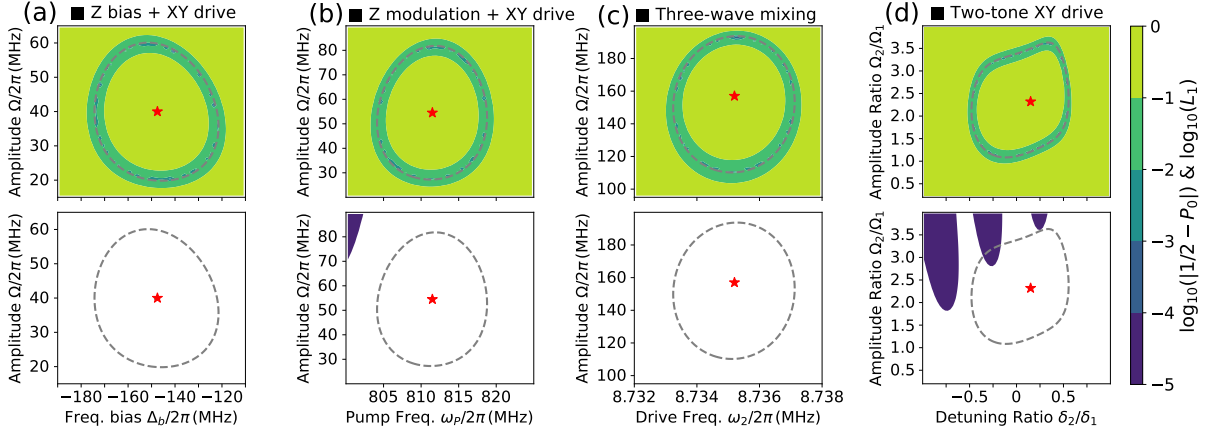


FIG. 5: The numerical verification of the four single-qubit gate schemes. In the numerical analysis, the transmon qubit is treated as an anharmonic oscillator [53] with the (maximum) frequency of  $\omega_q/2\pi = 5.25$  GHz and the anharmonicity of  $\eta_q/2\pi = -250$  MHz. The upper panel shows the population  $P_0$  at the end of the applied gate pulses depicted in Fig. 4, with the qubit prepared in state  $|0\rangle$ , while the bottom panel illustrates the leakage  $L_1$  (white regions indicate leakage below  $10^{-5}$ ). Dashed grey lines indicate the available regions for realizing  $\sqrt{X}$  gates while the red star is for  $X$  gates. (a)  $P_0$  and  $L_1$  versus the peak drive amplitude  $\Omega$  of the DRAG pulse (with a frequency of  $\omega_d/2\pi = 5.10$  GHz) and the frequency bias  $\Delta_b = \omega_q - \omega_d$ . (b)  $P_0$  and  $L_1$  versus the parametric drive frequency  $\omega_p$  and the microwave drive amplitude  $\Omega$  with the drive frequency of  $\omega_d/2\pi = 5.75$  GHz. Here, the dependence of qubit frequency on the flux bias is approximated by  $\omega(\Phi) = (\omega_q - \eta_q)\sqrt{|\cos(\pi\Phi/\Phi_0)|} + \eta_q$  [53], where  $\Phi_0$  denotes the flux quantum. The used parametric drive is  $\Phi = 0.05\Phi_0 + \Phi_p(t)\Phi_0 \cos(\omega_p t + \phi_0)$  (for simplicity, here  $\phi_0 = 0$ ) with a peak drive amplitude of  $\Phi_p = 0.2$ . The result shows the first-order sideband transition with  $\omega_p \sim |\omega_d - \omega_q|$ . (c)  $P_0$  and  $L_1$  versus the peak drive amplitudes  $\Omega$  of the two pulses and the frequency of the second drive  $\omega_2$ . The frequency of the first drive is  $\omega_1/2\pi = 3.5$  GHz. Here, the flux qubit is modeled as a qutrit with cycle transitions ( $\omega_{01}/2\pi = 6.25$  GHz,  $\omega_{02}/2\pi = 10$  GHz,  $\omega_{12}/2\pi = 3.75$  GHz) and transmon-flux coupling strength ( $g_{01}/2\pi = 94$  MHz,  $g_{02}/2\pi = 140$  MHz,  $g_{12}/2\pi = 136$  MHz) [58]. (d)  $P_0$  and  $L_1$  versus the drive amplitude ratio  $\Omega_2/\Omega_1$  and the drive-qubit detuning ratio  $\delta_2/\delta_1$  of the two pulses, where  $\delta_{1(2)} = \omega_{1(2)} - \omega_q$ . Here, for the first drive, the peak drive parameters and the drive-qubit detuning are  $\Omega_1/2\pi = 15$  MHz and  $\delta_1/2\pi = 50$  MHz, respectively.

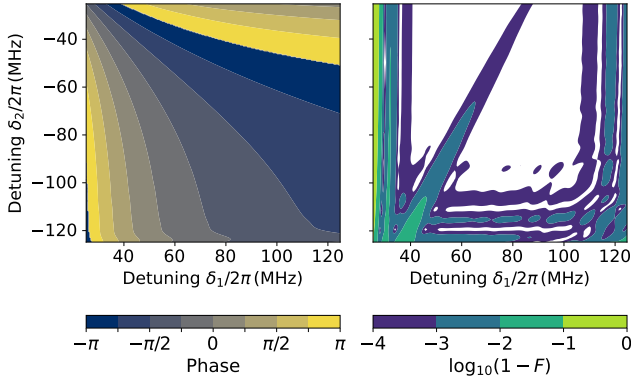


FIG. 6: Single-qubit Z gates. Z gates can be obtained by utilizing two off-resonance drives. Similar to Fig. 4(c), two 150-ns flat-top pulses with a ramp time of 50 ns are utilized. The left panel shows the angles of the Z rotation versus the two drive-qubit detunings  $\delta_1$  and  $\delta_2$ . Meanwhile, the associated Z gate error is shown in the right panel, with white regions indicating gate errors below  $10^{-4}$ .

The main reason for taking this compiling method is twofold. First, we prefer the  $\sqrt{X}$  gate rather than the  $X$  gate due to that the former one can provide more flexibility in choosing

control parameters. This flexibility could provide potential adaptations to address challenges involving inhomogeneities in coupling efficiencies between qubits and control lines, defects affecting qubit performance [37], frequency crowding in choosing control frequencies, and so on. Second, as control pulses are shared by qubits, individual Z gate applied to each qubit cannot be directly realized by the phase shift of the shared microwave drive or parametric drive [44, 74], especially in the gate schemes of (ST1), (ST2), and (SF2). Besides the two main reason, single-qubit errors, that result from microwave crosstalk, could be mitigated by optimizing the Z gates [75, 76] in this decomposition.

For the gate scheme of (SF1) based on the tree-wave mixing process, the phase of the effective drive applied to the qubit can be controlled by the difference phase or sum phase of the two pulses. Thus, in principle, the virtual Z gates can be utilized here. However, as mentioned above, the gate schemes of (ST1), (ST2), and (SF2) necessitate physical Z gates. Generally, this can be realized by using the ac-Stark effect due to off-resonance drives [77]. Here, we consider the implementation of arbitrary Z gates within (SF2), where two off-resonance microwave drive pulses are applied to the qubit. Similar to Fig. 4(c), a pair of raised cosine flat-top pulses are employed for performing Z rotations. Figures 6(a) and 6(b) show the Z rotation angle and the gate fidelity [78] versus the two drive-qubit detunings, respectively, illustrating that arbitrary Z rota-

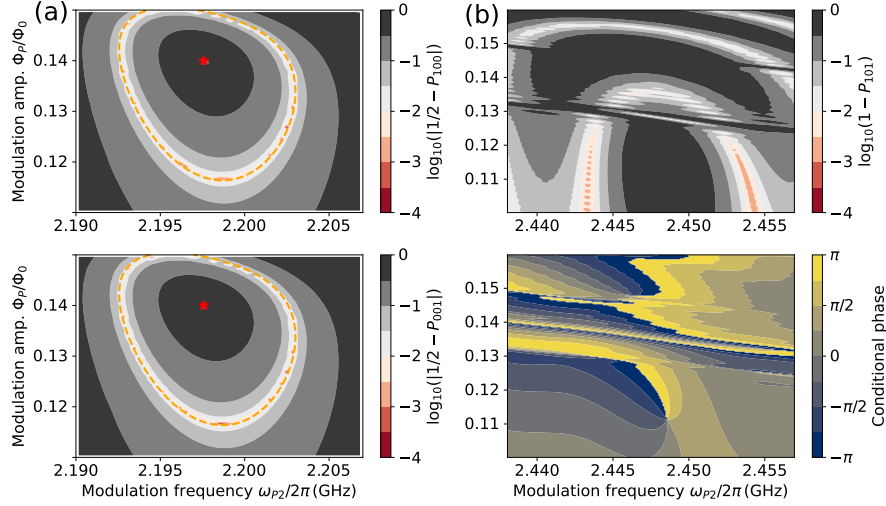


FIG. 7: The numerical verification of the two-qubit gate operations based on two-tone flux modulations. In the numerical analysis, we consider that two transmon qubits, labeled by  $Q_a$  and  $Q_b$ , are coupled via a tunable bus, labeled by  $Q_{bus}$ , and the system state is denoted by  $|Q_a Q_{bus} Q_b\rangle$ . The qubit frequencies are  $\omega_{a(b)}/2\pi = 5.05(5.25)$  GHz and the qubit anharmonicity is  $\eta_{a(b)}/2\pi = -250$  MHz. The maximum frequency and the anharmonicity of the tunable bus are  $\omega_{bus}/2\pi = 6.20$  GHz and  $\eta_{bus}/2\pi = -200$  MHz, respectively. The qubit-bus coupling strength is  $g/2\pi = 100$  MHz. The dependence of bus frequency on the two-tone flux modulation is approximated by  $\omega_{bus}(\Phi) = (\omega_{bus} - \eta_{bus})\sqrt{|\cos(\pi\Phi(t)/\Phi_0)|} + \eta_{bus}$  with  $\Phi(t) = \Phi_p(t)[\sin(\omega_{p1}t) + \sin(\omega_{p2}t + \phi_0)]$  (where  $\phi_0 = 0$  for simplicity) and the modulation frequency  $\omega_{p1}/2\pi = 2.0$  GHz. Here, similar to Fig. 4(c), two raised cosine flat-top pulses are used and the peak modulation amplitude is  $\Phi_p$ . (a) Population  $P_{100}$  (upper panel) and  $P_{001}$  (bottom panel) versus the modulation amplitude  $\Phi_p$  and the modulation frequency  $\omega_{p2}$  with the qubit prepared in state  $|100\rangle$ . The ramp time is 15 ns and the total gate length is 100 ns. Dashed orange lines indicate the available regions for realizing  $\sqrt{i}$ SWAP gates while the red star is for iSWAP gates. Here, the two-qubit gate is actuated when the difference frequency of the two modulations matches the qubit-qubit detuning. (b) Population  $P_{101}$  (upper panel) versus the modulation amplitude  $\Phi_p$  and the modulation frequency  $\omega_{p2}$  with the system prepared in state  $|101\rangle$ . The bottom panel shows the associated conditional phase. The ramp time is 25 ns and the total gate length is 200 ns. Here, the CZ gate is realized when the difference frequency of the two modulations matches the detuning between the energy levels of  $|101\rangle$  and  $|200\rangle$ . Note that discontinuities near the horizontal line at  $\Phi_p/\Phi_0 = 0.13$  arise from the parasitic interaction between the energy levels of  $|101\rangle$  and  $|110\rangle$ .

tions can be realized with high fidelity. Note here that while similar to the gate scheme of (F1) the phase difference can be controlled, the nonlinear dependence of the qubit dynamics on the frequency difference or phase difference makes it incompatible with the virtual Z scheme [59], see Appendix A for details.

## B. Two-qubit gates

As discussed in Sec. II, to be compatible with the multiplexed control architecture, we consider two-qubit gates based on driving single qubit or a coupler in two-coupled qubit systems. Table II summarizes three possible two-qubit gate schemes supporting the row-column addressing:

(DT1) For two fixed-frequency qubits coupled via a coupler (bus), two-qubit gates can be obtained by only tuning the coupler (bus) frequency [79–83]. Given the shared flux pulses, each coupler (bus) can be individually tuned by using the on-chip programmable magnetic memory [30, 31, 37], as shown in Fig. 3(a). Note that with the help of local memory, in principle, only Z lines shared by the couplers or buses are needed to perform parallel two-qubit gates.

TABLE II: Two-qubit schemes with two control pulses. Similar to the qubit addressing, note that for two-qubit gates based on frequency-tunable coupler or bus, static dc flux biases (not listed here) are generally needed for biasing the coupler or bus at their idle points. This can be achieved by using an on-chip programmable magnetic memory, as shown in the left inset of Fig. 3(a).

Specific	Two-qubit addressing strategy
Tunable element	(DT1) Baseband flux pulse + local memory [37];
	(DT2) Two-tone flux modulation;
Fixed element	(DF1) Frequency mixer: e.g. three-wave mixing [55–58];

(DT2) By leveraging the nonlinear dependence of the transmon qubit or transmon coupler frequency on the flux bias, two-qubit gates can be realized by applying two-tone flux modulations on the qubits or the coupler. When the the sum or difference frequency of the two modulations match the subharmonic of the qubit-qubit detuning, two-qubit gates can be actuated. For example, considering two fixed-frequency transmon qubits coupled via tunable bus [47], Figure 7 shows that two-qubit gates, such as iSWAP,  $\sqrt{i}$ SWAP, and CZ gates can

be obtained by the two-tone modulation of the bus frequency. This two-tone modulation scheme is adaptable to other coupler circuits [48–50]. In Appendix B, we further show that two-qubit gates can be obtained by applying the two-tone flux modulation to one of the coupled qubits.

(DF1) For two-qubit gates based on driving a single qubit, the three-wave mixer could be used to generate the desired effective single-qubit drive. However, considering the existing techniques [55–58], the strength of the effective drive (here the strength is about  $\sim 1$  MHz) is too weak to support the successful implementation of microwave-activated two-qubit gates, such as cross-resonance (CR) gates [45]. Therefore, new physical components that enable the three-wave mixing process should be introduced to generate effective drives with large amplitudes.

Given the above discussions, the scheme of (DT2) emerges as the most viable option among the three schemes, whereas the scheme of (DF1) poses the greatest challenge, necessitating the demonstration of new physical components. In addition to the three discussed schemes, similar to the single-qubit gate scheme of (SF2), two-qubit gates, which are actuated by applying two-tone microwave drives to a qubit or a coupler, should be potential solutions for supporting the row-column addressing and are thus worth exploring in future works.

#### IV. CHALLENGES TOWARDS LARGE-SCALE MULTIPLEXED CONTROL ARCHITECTURES

In state-of-the-art superconducting quantum processors, several issues, such as distortions in control signals [84, 85], crosstalk among control signals [7], and temporal fluctuations of qubit parameters and coherence times (due to factors like two-level systems) [86], are not yet to be well addressed for achieving reliable, accurate quantum computing. This becomes even more challenging within the multiplexed control architecture.

To be more specific, currently, independent control allows various active approaches to be employed for alleviating the detrimental effects of these issues on qubits. However, due to the control limitations, these approaches cannot be directly applied to address similar issues within the multiplexed control architecture. Consequently, rather than merely attempting to calibrate away these issues, instead, one might turn to fully suppress or eliminate these issues at the qubit chip level. Nevertheless, given state-of-the-art technologies, significant advancements in this regard is unlikely to be achieved soon. Additionally, at the level of control pulses, robust quantum control could be explored to provide resilience against these issues [87], while at the circuit level, gate compilations with adaptations to address these issues can be developed [75, 76].

In addition to the aforementioned well-recognized hurdles, there exist two new challenges that are particularly important in achieving high-fidelity qubit control within the multiplexed control architecture but are rarely involved in the traditional independent control architecture. In the following, we will discuss the two challenges to be faced when considering scaling up the multiplexed control architecture.

#### A. The non-uniformity of qubit parameters

As illustrated in Sec. II and Sec. III, here the gate pulses are shared by multiple qubits, thus the gate condition for each qubit is distinctively intertwined with each other. For clarity, we assume that the coupling efficiencies between control lines and qubits are all the same and focus on the single-qubit gates (similar results can also be obtained for the two-qubit gates discussed in Sec. III B). In the single-qubit gate schemes illustrated in Sec. III A, with fixed-length drives featuring the same pulse shape, gates can only be actuated when the gate conditions

$$F(\Omega_i, \Omega_j, \omega_i, \omega_j) = \omega_{ij} \quad (1)$$

are satisfied. Here  $\Omega_i$  ( $\Omega_j$ ) and  $\omega_i$  ( $\omega_j$ ) denote the amplitude and frequency of the two drive pulses applied to the qubit (with the frequency of  $\omega_{ij}$ ), which is located at the intersection of the  $i$ th row line and the  $j$ th column line. As mentioned in Sec. III A, in the following, we focus on  $\sqrt{X}$  gates, which provide more flexibility in setting pulse parameters (similarly, for two-qubit gates, one might prefer  $\sqrt{CZ}$  gates [38] or  $\sqrt{i}$ SWAP gates, see, e.g., Fig. 7).

Under the condition of Eq. (1) and given fixed drive amplitudes, pulse solutions for the scheme, which relies on the resonance condition  $f(\omega_i, \omega_j) = \omega_{ij}$  (see, e.g., Fig. 8 in Appendix A), such as (SF2), (ST1), and (ST2), can in principle exist. This is because in a square qubit lattice comprising  $n \times n$  qubits,  $2n$  distinct frequencies should suffice for actuating parallel gate operations. However, even if solutions exist, considering that the resonance conditions are generally intertwined with the drive amplitudes and the non-uniformity of qubit parameters, such as the coupling efficiency between qubits and control lines (i.e., leading to the non-uniformity of the drive amplitude), are ubiquitous in reality, whether and how such solutions can be realized practically in large-scale systems should be open questions. This issue warrants further exploration in future works. In the following, we also consider an alternative approach, i.e., reducing the number of conditions, allowing us to explore another extreme ('trivial') situation.

In the context of 2D square qubit lattices depicted in Fig. 2(a), the utilization of two sets of shared row-column lines allow us to selectively address neighboring qubits, i.e., data qubits and syndrome qubits. In this way, the qubit frequency allocation in each diagonal can follow a zigzag pattern, e.g., where data qubits at a frequency band with a typical value of  $\omega_D$  and syndrome qubits at a separate frequency band with a typical value of  $\omega_S$ . Consequently, the gate conditions for data qubits and syndrome qubits are decoupled to each other, facilitating a separate treatment for each type of qubits. Hence, in the following, we focus on the data qubits with gate conditions potentially being reduced to a single criterion denoted by

$$F(\Omega_{D,i}, \Omega_{D,j}, \omega_{D,i}, \omega_{D,j}) = \omega_{D,ij} \simeq \omega_D, \quad (2)$$

where the subscript  $D$  indicates the gate condition for data qubits. Finding the solution of the above equation is equiva-



lent to control of an ensemble of qubits, where the qubit frequencies could be different from qubit to qubit (given state-of-the-art technologies [88, 89], the non-uniformity of qubit frequency can be suppressed to the level of 10 MHz [88]), using uniform control pulses, i.e., the parameters of the pulse in each row or column are the same.

However, in fact, besides the qubit frequency and the coupling efficiency, the non-uniformity of qubit parameters also results from other factors, such as the qubit anharmonicity and the phase difference among control lines. Therefore, considering all these non-uniformity of qubit parameters, whether one can find the pulse solution of Eq. (2) for multiplexed control of large-scale qubit systems crucially hinges on the uniformity of qubit parameters. Furthermore, if these non-uniformity issues can be effectively addressed, the multiplexed control can be simplified to a trivial situation, eliminating the need for row-column addressing and two-pulse control configurations.

As shown in Fig. 3(a), in principle, on-chip programmable magnetic memory can be used to mitigate most of the above-discussed non-uniform issues [30, 37] but its compatibility with high-fidelity qubit control has not yet been demonstrated. Meanwhile, robust quantum control could also be explored to optimize the control pulse against these non-uniformity issues [87, 90, 91]. Given state-of-the-art quantum technologies and the above discussions, we expect that solely adopting one of the two types of gate solutions supporting the gate conditions in Eqs. (1) and (2) presents a formidable hurdle in achieving high-fidelity multiplexed qubit control at scale. Therefore, one might choose to take the combination of such two solutions, thus enabling the adaptations to address various issues, including the non-uniformity issue.

### B. Gate calibration

While individual gate calibrations and benchmarking may still be possible as in the independent control architecture [92, 93], the multiplexed control should lead to a significant degradation of the efficiency and the performance that can be reached. This is because that the gate calibration procedures for each qubit are intertwined with each other. Alternatively, one might also consider fine-tuning up gates at the quantum circuit level, such as stabilize measurement circuits [94], where the detection events can be used for informing and guiding the optimization of gate parameters.

Moreover, when calibrating gate parameters tailored to implement distinct gates on individual qubits, additional overhead is required. As illustrated in Fig. 2(a), given the  $\sqrt{X}$  gates, arbitrary single-qubit gates, including identity operations, can be directly optimized by tuning up the Z gates. However, as discussed in Sec. II, selectively activating two-qubit gates on qubit subgroups, such as implementing standard two-qubit gates (e.g., iSWAP-type gates and CZ gates) on selective qubits while applying identity operations to the inactive qubits, presents a nontrivial task for gate tune-up.

These challenges generally stem from the tradeoff between line overhead and control flexibility. In order to compensate for the degradation in control flexibility, additional gates or

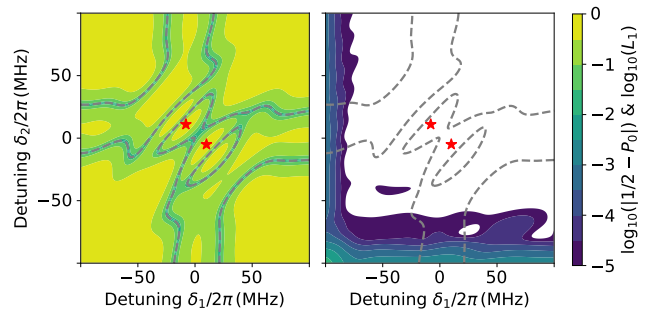


FIG. 8: Nonlinear dependence on the frequency difference of the two-tone microwave drive. The left (right) panel shows the population  $P_0$  (the leakage  $L_1$ ) versus the drive-qubit detunings  $\delta_1$  and  $\delta_2$  (white regions are where leakage below  $10^{-5}$ ). Here, the peak drive parameters are  $\Omega_{1(2)}/2\pi = 25\text{MHz}$ . Dashed grey lines indicate the feasible regions for realizing  $\sqrt{X}$  gates while the red stars indicate the gate parameters for implementing X gates.

gate patterns need to be tuned up, potentially leading to an increase in circuit depths [42].

## V. CONCLUSION

In conclusion, we introduce a multiplexed control architecture for superconducting qubits with shared row-column lines. This architecture could in principle provide an efficient approach for parallel controlling  $N$  qubits with  $O(\sqrt{N})$  control lines. We also propose various single- and two-qubit gate schemes that are both compatible with the row-column qubit addressing scheme and the existing superconducting qubit technologies. Leveraging the inherent parallelism of this architecture, we show that the multiplexed control is suitable for the implementation of structured quantum circuits. As an immediate application, we show that the architecture can be specifically tailored to execute the quantum error correction with surface code.

We envision that a proof-of-concept demonstration of multiplexed qubit control on a small scale could be feasible with the current technologies and hope that our work could motivate further experimental and theoretical research in incorporating shared control into scalable quantum information processing with superconducting qubits.

### Acknowledgments

The author would like to thank Guangming Xue, Jun Li, Kunzhe Dai, Zhikun Han, and Fei Yan for the insightful discussions. Thanks also go to Peng Xu, Dong Lan, and Haifeng Yu for their generous support. The author also gratefully acknowledges support from the National Natural Science Foundation of China (Grants No.12204050) and the Beijing Academy of Quantum Information Sciences.

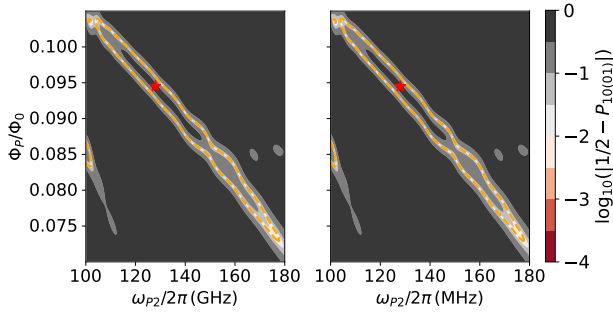


FIG. 9: The two-qubit gate operations based on applying two-tone flux modulations to qubits. We consider that two transmon qubits, labeled by  $Q_a$  and  $Q_b$ , are coupled directly and a two-tone flux modulation is applied to the frequency-tunable qubit  $Q_a$ . The system state is denoted by  $|Q_a Q_b\rangle$ . The left (right) panel shows population  $P_{10}$  ( $P_{01}$ ) versus the modulation amplitude  $\Phi_p$  and the modulation frequency  $\omega_{p2}$  with the system prepared in state  $|10\rangle$ . Dashed orange lines indicate the available regions for realizing  $\sqrt{i}$ SWAP gates while the red star is for iSWAP gates.

#### Appendix A: Nonlinear dependence on the frequency difference in the two-tone drive scheme

For the two-tone microwave drives of (SF2) studied in Fig. 3(d), Figure 8 shows the population  $P_0$  and the leakage

$L_1$  versus the drive-qubit detunings  $\delta_1$  and  $\delta_2$ , demonstrating the nonlinear dependence of the single-qubit dynamics on the frequency difference of the two drives. Here, as in Fig. 3, in the numerical analysis, the qubit frequency and the anharmonicity are  $\omega_q/2\pi = 5.25$  GHz and  $\eta_q/2\pi = -250$  MHz, respectively.

#### Appendix B: iswap gates using two-tone flux modulation of qubits

Here, we consider that one frequency-tunable transmon qubit, labeled by  $Q_a$ , is coupled fixedly to a fixed-frequency transmon qubit, labeled by  $Q_b$ , with the coupling strength of  $g/2\pi = 5.5$  MHz. The qubit frequencies and the qubit anharmonicities are  $\omega_{a(b)}/2\pi = 5.05(5.25)$  GHz and  $\eta_{a(b)}/2\pi = 250$  MHz, respectively. When applying the two-tone flux modulation to  $Q_a$ , the qubit frequency is approximated by  $\omega_a(\Phi) = (\omega_a - \eta_a) \sqrt{|\cos(\pi\Phi(t)/\Phi_0)|} + \eta_a$  with  $\Phi(t) = \Phi_p(t)[\sin(\omega_{p1}t) + \sin(\omega_{p2}t + \phi_0)]$ . Here, the modulation frequency is  $\omega_{p1}/2\pi = 50$  MHz and  $\phi_0 = 0$  for simplicity. As in Fig. 7(a), the raised cosine flat-top pulses are used, with a total gate length of 100 ns and a ramp time of 15 ns. Figure 9 demonstrates that under such a two-tone flux modulation, two-qubit gates, such as  $\sqrt{i}$ SWAP gates and iSWAP gates, can be actuated.

- 
- [1] B. M. Terhal, Quantum Error Correction for Quantum Memories, *Rev. Mod. Phys.* **87**, 307 (2015).
  - [2] E. Dennis, A. Kitaev, A. Landahl, and J. Preskill, Topological quantum memory, *J. Math. Phys.* **43**, 4452-4505 (2002).
  - [3] E. Campbell, A series of fast-paced advances in Quantum Error Correction, *Nat. Rev. Phys.* (2024).
  - [4] S. Krinner, N. Lacroix, A. Remm, A. D. Paolo, E. Genois, C. Leroux, C. Hellings, S. Lazar, F. Swiadek, J. Herrmann, G. J. Norris, C. K. Andersen, M. Müller, A. Blais, C. Eichler, and A. Wallraff, Realizing repeated quantum error correction in a distance-three surface code, *Nature* **605**, 669-674 (2022).
  - [5] Y. Zhao, Y. Ye, H.-L. Huang, Y. Zhang, D. Wu, H. Guan, Q. Zhu, Z. Wei, T. He, S. Cao *et al.*, Realization of an Error-Correcting Surface Code with Superconducting Qubits, *Phys. Rev. Lett.* **129**, 030501 (2022).
  - [6] N. Sundaresan, T. J. Yoder, Y. Kim, M. Li, E. H. Chen, G. Harper, T. Thorbeck, A. W. Cross, A. D. Córcoles, and M. Takita, Demonstrating multi-round subsystem quantum error correction using matching and maximum likelihood decoders, *Nat. Commun.* **14**, 2852 (2023).
  - [7] Q. Acharya, I. Aleiner, R. Allen, T. I. Andersen, M. Ansmann, F. Arute, K. Arya, A. Asfaw, J. Atalaya, R. Babbush *et al.*, Suppressing Quantum Errors by Scaling a Surface Code Logical Qubit, *Nature (London)* **614**, 676 (2023).
  - [8] A. G. Fowler, M. Mariantoni, J. M. Martinis, and A. N. Cleland, Surface codes: Towards practical large-scale quantum computation, *Phys. Rev. A* **86**, 032324 (2012).
  - [9] A. Gidney and M. Ekerå, How to factor 2048 bit RSA integers in 8 hours using 20 million noisy qubits, *Quantum* **5**, 433 (2021).
  - [10] Z. Chen, Metrology of Quantum Control and Measurement in Superconducting Qubits, Ph.D. thesis. University of California, Santa Barbara, 2018.
  - [11] S. Krinner, S. Storz, P. Kurpiers, P. Magnard, J. Heinsoo, R. Keller, J. Lütolf, C. Eichler, and A. Wallraff, Engineering cryogenic setups for 100-qubit scale superconducting circuit systems, *EPJ Quantum Technology* **6**, 2 (2019).
  - [12] P. Krantz, M. Kjaergaard, F. Yan, T. P. Orlando, S. Gustavsson, and W. D. Oliver, A Quantum Engineer's Guide to Superconducting Qubits, *Appl. Phys. Rev.* **6**, 021318 (2019).
  - [13] D. P. Franke, J. S. Clarke, L. M. K. Vandersypen, and M. Veldhorst, Rent's rule and extensibility in quantum computing, *Microprocess. Microsy.* **67**, 1 (2019).
  - [14] L. M. K. Vandersypen, H. Bluhm, J. S. Clarke, A. S. Dzurak, R. Ishihara, A. Morello, D. J. Reilly, L. R. Schreiber, and M. Veldhorst, Interfacing spin qubits in quantum dots and donors-hot, dense, and coherent, *npj Quantum Inf.* **3**, 34 (2017).
  - [15] D. J. Reilly, Challenges in Scaling-up the Control Interface of a Quantum Computer, *2019 IEEE International Electron Devices Meeting (IEDM)*, 31.7 (2019).
  - [16] J. M. Martinis, Information Constraints for Scalable Control in a Quantum Computer, *arXiv:2012.14270*.
  - [17] S. Asaad, C. Dickel, S. Poletto, A. Bruno, N. K. Langford, M. A. Rol, D. Deurloo, and L. DiCarlo, Independent, extensible control of same-frequency superconducting qubits by selective broadcasting, *npj Quantum Inf.* **2**, 16029 (2016).
  - [18] F. Lecocq, F. Quinlan, K. Cicak, J. Aumentado, S. A. Diddams, and J. D. Teufel, Control and readout of a superconducting qubit

- using a photonic link, *Nature* **591**, 575-579 (2021).
- [19] R. McDermott, M. G. Vavilov, B. L. T. Plourde, F. K. Wilhelm, P. J. Liebermann, O. A. Mukhanov, and T. A. Ohki, Quantum-classical interface based on single flux quantum digital logic, *Quantum Sci. Technol.* **3**, 024004 (2018).
- [20] J. C. Bardin, E. Jeffrey, E. Lucero, T. Huang, S. Das, D. T. Sank, O. Naaman, A. E. Megrant, R. Barends, T. White *et al.*, Design and Characterization of a 28-nm Bulk-CMOS Cryogenic Quantum Controller Dissipating Less Than 2 mW at 3 K, *IEEE Journal of Solid-State Circuits* **54**, 3043 (2019).
- [21] J. P. G. Van Dijk, B. Patra, S. Subramanian, X. Xue, N. Samkharadze, A. Corna, C. Jeon, F. Sheikh, E. Juarez-Hernandez, B. P. Esparza *et al.*, A scalable cryoCMOS controller for the wideband frequency-multiplexed control of spin qubits and transmons, *IEEE Journal of Solid-State Circuits* **55**, 2930 (2020).
- [22] S. Chakraborty, D. J. Frank, K. Tien, P. Rosno, M. Yeck, J. A. Glick, R. Robertazzi, R. Ricketta, J. F. Bulzacchelli, D. Underwood *et al.*, A cryo-CMOS low-power semi-autonomous transmon qubit state controller in 14-nm FinFET technology, *IEEE Journal of Solid-State Circuits* **57**, 3258 (2022).
- [23] N. Takeuchi, T. Yamae, W. Luo, F. Hirayama, T. Yamamoto, and N. Yoshikawa, Scalable flux controllers using adiabatic superconductor logic for quantum processors, *Phys. Rev. Research* **5**, 013145 (2023).
- [24] N. Takeuchi, T. Yamae, T. Yamashita, T. Yamamoto, and N. Yoshikawa, Scalable quantum-bit controller using adiabatic superconductor logic, [arXiv:2310.06544](https://arxiv.org/abs/2310.06544).
- [25] R. Acharya, S. Brebels, A. Grill, J. Verjauw, Ts. Ivanov, D. Perez Lozano, D. Wan, J. Van Damme, A. M. Vadiraj, M. Mongillo, B. Govoreanu, J. Craninckx, I. P. Radu, K. De Greve, G. Gielen, F. Cathoor, and A. Potočník, Multiplexed superconducting qubit control at millikelvin temperatures with a low-power cryoCMOS multiplexer, *Nat. Electron.* **6**, 900-909 (2023).
- [26] C.H. Liu, A. Ballard, D. Olaya, D.R. Schmidt, J. Biesecker, T. Lucas, J. Ullom, S. Patel, O. Rafferty, A. Opremcak, K. Dodge, V. Iai, T. McBroom, J.L. DuBois, P.F. Hopkins, S.P. Benz, B.L.T. Plourde, and R. McDermott, Single Flux Quantum-Based Digital Control of Superconducting Qubits in a Multi-chip Module, *PRX Quantum* **4**, 030310 (2023).
- [27] C. D. Hill, E. Peretz, S. J. Hile, M. G. House, M. Fuechsle, S. Rogge, M. Y. Simmons, and L. C. L. Hollenberg, A surface code quantum computer in silicon, *Sci. Adv.* **1**, e1500707 (2015).
- [28] M. Veldhorst, H. G. J. Eenink, C. H. Yang, and A. S. Dzurak, Silicon CMOS architecture for a spin-based quantum computer, *Nat. Commun.* **8**, 1766 (2017).
- [29] R. Li, L. Petit, D. P. Franke, J. P. Dehollain, J. Helsen, M. Steudtner, N. K. Thomas, Z. R. Yoscovits, K. J. Singh, S. Wehner *et al.*, A Crossbar Network for Silicon Quantum Dot Qubits, *Sci. Adv.* **4**, eaar3960 (2018).
- [30] M. W. Johnson, P. Bunyk, F. Maibaum, E. Tolkacheva, A. J. Berkley, E. M. Chapple, R. Harris, J. Johansson, T. Lanting, and I. Perminov *et al.*, A Scalable Control System for a Superconducting Adiabatic Quantum Optimization Processor, *Supercond. Sci. Technol.* **23**, 065004 (2010).
- [31] P. I. Bunyk, E. M. Hoskinson, M. W. Johnson, E. Tolkacheva, F. Altomare, A. J. Berkley, R. Harris, J. P. Hilton, T. Lanting, A. J. Przybysz *et al.*, Architectural considerations in the design of a superconducting quantum annealing processor, *IEEE Trans. Appl. Supercond.* **24**, 1700110 (2014).
- [32] M. Jerger, S. Poletto, P. Macha, U. Hübner, A. Lukashenko, E. Il'ichev, and A. V. Ustinov, Readout of a qubit array via a single transmission line, *Europhys. Lett.* **96**, 40012 (2011).
- [33] M. Jerger, S. Poletto, P. Macha, U. Hübner, E. Il'ichev, and A. V. Ustinov, Frequency division multiplexing readout and simultaneous manipulation of an array of flux qubits, *Appl. Phys. Lett.* **101**, 042604 (2012).
- [34] Y. Chen, D. Sank, P. O'Malley, T. White, R. Barends, B. Chiaro, J. Kelly, E. Lucero, M. Mariantoni, A. Megrant, C. Neill, A. Vainsencher, J. Wenner, Y. Yin, A. N. Cleland, and John M. Martinis, Multiplexed dispersive readout of superconducting phase qubits, *Appl. Phys. Lett.* **101**, 182601 (2012).
- [35] D.-Y. Li, J. Chu, W. Zheng, D. Lan, J. Zhao, S.-X. Li, X.-S. Tan, and Y. Yu, Universal quantum control based on parametric modulation in superconducting circuits, *Chin. Phys. B* **30**, 070308 (2021).
- [36] J. H. Béjanin, C. T. Earnest, and M. Mariantoni, The Quantum Socket and DemuXYZ-Based Gates with Superconducting Qubits, [arXiv:2211.00143](https://arxiv.org/abs/2211.00143).
- [37] P. Zhao, R. Wang, M.-J. Hu, T. Ma, P. Xu, Y. Jin, and H. Yu, Baseband Control of Superconducting Qubits with Shared Microwave Drives, *Phys. Rev. Appl.* **19**, 054050 (2023).
- [38] P. Shi, J. Yuan, F. Yan, and H. Yu, Multiplexed control scheme for scalable quantum information processing with superconducting qubits, [arXiv:2312.06911](https://arxiv.org/abs/2312.06911).
- [39] Z. György, A. Pályi, and G. Széchenyi, Electrically driven spin resonance with bichromatic driving, *Phys. Rev. B* **106**, 155412 (2022).
- [40] S. Bosco, S. Geyer, L. C. Camenzind, R. S. Eggli, A. Fuhrer, R. J. Warburton, D. M. Zumbühl, J. C. Egues, A. V. Kuhlmann, and D. Loss, Phase driving hole spin qubits, [arXiv:2303.03350](https://arxiv.org/abs/2303.03350).
- [41] V. John, F. Borsoi, Z. György, C.-A. Wang, G. Széchenyi, F. v. Riggelen, W. I. L. Lawrie, N. W. Hendrickx, A. Sammak, G. Scappucci, A. Pályi, and M. Veldhorst, Bichromatic Rabi control of semiconductor qubits, [arXiv:2308.01720](https://arxiv.org/abs/2308.01720).
- [42] D. B. Tan, S. Ping, and J. Cong, Depth-Optimal Addressing of 2D Qubit Array with 1D Controls Based on Exact Binary Matrix Factorization, [arXiv:2401.13807](https://arxiv.org/abs/2401.13807).
- [43] Z. Han, C. Lyu, Y. Zhou, J. Yuan, J. Chu, W. Nuerbolati, H. Jia, L. Nie, W. Wei, Z. Yang *et al.*, Multilevel variational spectroscopy using a programmable quantum simulator, *Phys. Rev. Research* **6**, 013015 (2024).
- [44] D. C. McKay, C. J. Wood, S. Sheldon, J. M. Chow, and J. M. Gambetta, Efficient Z gates for quantum computing, *Phys. Rev. A* **96**, 022330 (2017).
- [45] J. M. Chow, A. D. Córcoles, J. M. Gambetta, C. Rigetti, B. R. Johnson, J. A. Smolin, J. R. Rozen, G. A. Keefe, M. B. Rothwell, M. B. Ketchen, and M. Steffen, Simple All-Microwave Entangling Gate for Fixed-Frequency Superconducting Qubits, *Phys. Rev. Lett.* **107**, 080502 (2011).
- [46] S. A. Caldwell, N. Didier, C. A. Ryan, E. A. Sete, A. Hudson, P. Karalekas, R. Manenti, M. P. da Silva, R. Sinclair, E. Acala *et al.*, Parametrically Activated Entangling Gates Using Transmon Qubits, *Phys. Rev. Appl.* **10**, 034050 (2018).
- [47] D. C. McKay, S. Filipp, A. Mezzacapo, E. Magesan, J. M. Chow, and J. M. Gambetta, Universal gate for fixed-frequency qubits via a tunable bus, *Phys. Rev. Applied* **6**, 064007 (2016).
- [48] P. S. Mundada, G. Zhang, T. Hazard, and A. A. Houck, Suppression of Qubit Crosstalk in a Tunable Coupling Superconducting Circuit, *Phys. Rev. Applied* **12**, 054023 (2019).
- [49] X. Y. Han, T. Q. Cai, X. G. Li, Y. K. Wu, Y. W. Ma, Y. L. Ma, J. H. Wang, H. Y. Zhang, Y. P. Song, and L. M. Duan, Error analysis in suppression of unwanted qubit interactions for a parametric gate in a tunable superconducting circuit, *Phys. Rev. A* **102**, 022619 (2020).
- [50] K. Kubo and H. Goto, Fast parametric two-qubit gate for

- highly detuned fixed-frequency superconducting qubits using a double-transmon coupler, *Appl. Phys. Lett.* **122**, 064001 (2023).
- [51] C. Horsman, A. G. Fowler, S. Devitt, and R. V. Meter, Surface code quantum computing by lattice surgery, *New J. Phys.* **14**, 123011 (2012).
- [52] A. G. Fowler and C. Gidney, Low overhead quantum computation using lattice surgery, [arXiv:1808.06709](https://arxiv.org/abs/1808.06709).
- [53] J. Koch, T. M. Yu, J. Gambetta, A. A. Houck, D. I. Schuster, J. Majer, A. Blais, M. H. Devoret, S. M. Girvin, and R. J. Schoelkopf, Charge-insensitive qubit design derived from the cooper pair box, *Phys. Rev. A* **76**, 042319 (2007).
- [54] V. E. Manucharyan, J. Koch, L. I. Glazman, and M. H. Devoret, Fluxonium: Single Cooper-pair circuit free of charge offsets, *Science* **326**, 113 (2009).
- [55] N. E. Frattini, U. Vool, S. Shankar, A. Narla, K. M. Sliwa, and M. H. Devore, 3-wave mixing Josephson dipole element, *Appl. Phys. Lett.* **110**, 222603 (2017).
- [56] B. J. Chapman, S. J. de Graaf, S. H. Xue, Y. Zhang, J. Teoh, J. C. Curtis, T. Tsunoda, A. Eickbusch, A. P. Read, A. Kootandavida, S. O. Mundhada, L. Frunzio, M.H. Devoret, S.M. Girvin, and R.J. Schoelkopf, High-On-Off-Ratio Beam-Splitter Interaction for Gates on Bosonically Encoded Qubits, *PRX Quantum* **4**, 020355 (2023).
- [57] Yu-xi Liu, H.-C. Sun, Z. H. Peng, A. Miranowicz, J. S. Tsai, and F. Nori, Controllable microwave three-wave mixing via a single three-level superconducting quantum circuit, *Sci Rep* **4**, 7289 (2014).
- [58] P. Zhao, Z. Jin, P. Xu, X. Tan, H. Yu, and Y. Yu, Two-Photon Driven Kerr Resonator for Quantum Annealing with Three-Dimensional Circuit QED, *Phys. Rev. Appl.* **10**, 024019 (2018).
- [59] K. Dai, H. Wu, P. Zhao, M. Li, Q. Liu, G. Xue, X. Tan, H. Yu, and Y. Yu, Quantum simulation of the general semi-classical Rabi model in regimes of arbitrarily strong driving, *Appl. Phys. Lett.* **111**, 242601 (2017).
- [60] Y.-M. He, H. Wang, C. Wang, M.-C. Chen, X. Ding, J. Qin, Z.-C. Duan, S. Chen, J.-P. Li, R.-Z. Liu *et al.*, Coherently driving a single quantum two-level system with dichromatic laser pulses, *Nat. Phys.* **15**, 941 (2019).
- [61] Z. X. Koong, E. Scerri, M. Rambach, M. Cygorek, M. BrotonsGisbert, R. Picard, Y. Ma, S. I. Park, J. D. Song, E. M. Gauger, and B. D. Gerardot, Coherent Dynamics in Quantum Emitters under Dichromatic Excitation, *Phys. Rev. Lett.* **126**, 047403 (2021).
- [62] T. K. Bracht, M. Cosacchi, T. Seidelmann, M. Cygorek, A. Vagov, V. M. Axt, T. Heindel, and D. E. Reiter, Swing-Up of Quantum Emitter Population Using Detuned Pulses, *PRX Quantum* **2**, 040354 (2021).
- [63] Z. T. Wang, P. Zhao, Z. H. Yang, Ye Tian, H. F. Yu, and S. P. Zhao, Escaping Detrimental Interactions with Microwave-Dressed Transmon Qubits, *Chin. Phys. Lett.* **40**, 070304 (2023).
- [64] F. Motzoi, J. M. Gambetta, P. Rebentrost, and F. K. Wilhelm, Simple Pulses for Elimination of Leakage in Weakly Nonlinear Qubits, *Phys. Rev. Lett.* **103**, 110501 (2009).
- [65] Z. Chen, J. Kelly, C. Quintana, R. Barends, B. Campbell, Y. Chen, B. Chiaro, A. Dunsworth, A. G. Fowler, E. Lucero, E. Jeffrey, A. Megrant, J. Mutus, M. Neeley, C. Neill, P. J. J. ÓMalley, P. Roushan, D. Sank, A. Vainsencher, J. Wenner, T. C. White, A. N. Korotkov, and J. M. Martinis, Measuring and Suppressing Quantum State Leakage in a Superconducting Qubit, *Phys. Rev. Lett.* **116**, 020501 (2016).
- [66] R. Harris, T. Lanting, A. J. Berkley, J. Johansson, M. W. Johnson, P. Bunyk, E. Ladizinsky, N. Ladizinsky, T. Oh, and S. Han, Compound Josephson-junction coupler for flux qubits with minimal crosstalk, *Phys. Rev. B* **80**, 052506 (2009).
- [67] Alec Maassen van den Brink, A. J. Berkley, and M. Yalowsky, Mediated tunable coupling of flux qubits, *New J. Phys.* **7**, 230 (2005).
- [68] R. Harris, A. J. Berkley, M. W. Johnson, P. Bunyk, S. Govorkov, M. C. Thom, S. Uchaikin, A. B. Wilson, J. Chung, E. Holtham, J. D. Biamonte, A. Yu. Smirnov, M. H. S. Amin, and Alec Maassen van den Brink, Sign- and Magnitude-Tunable Coupler for Superconducting Flux Qubits, *Phys. Rev. Lett.* **98**, 177001 (2007).
- [69] J. D. Strand, Matthew Ware, F. Beaudoin, T. A. Ohki, B. R. Johnson, A. Blais, and B. L. T. Plourde, First-order sideband transitions with flux-driven asymmetric transmon qubits, *Phys. Rev. B* **87**, 220505(R) (2013).
- [70] P. Zhao, T. Ma, Y. Jin, and H. Yu, Combating fluctuations in relaxation times of fixed-frequency transmon qubits with microwave-dressed states, *Phys. Rev. A* **105**, 062605 (2022).
- [71] T. K. Bracht, T. Seidelmann, Y. Karli, F. Kappe, V. Remesh, G. Weihs, V. M. Axt, and D. E. Reiter, Dressed-state analysis of two-color excitation schemes, *Phys. Rev. B* **107**, 035425 (2023).
- [72] I. Zuk, D. Cohen, A. V. Gorshkov, and A. Retzker, Robust gates with spin-locked superconducting qubits, [arXiv:2306.09149](https://arxiv.org/abs/2306.09149).
- [73] C. J. Wood and J. M. Gambetta, Quantification and characterization of leakage errors, *Phys. Rev. A* **97**, 032306 (2018).
- [74] J. Chen, D. Ding, C. Huang, and Q. Ye, Compiling arbitrary single-qubit gates via the phase shifts of microwave pulses, *Phys. Rev. Research* **5**, L022031 (2023).
- [75] R. Wang, P. Zhao, Y. Jin, and H. Yu, Control and mitigation of microwave crosstalk effect with superconducting qubits, *Appl. Phys. Lett.* **121**, 152602 (2022).
- [76] R. Wang, P. Zhao, and H. Yu, Universality of universal single-qubit-gate decomposition with coherent errors, [arXiv:2211.00365](https://arxiv.org/abs/2211.00365).
- [77] K. X. Wei, E. Pritchett, D. M. Zajac, D.C. McKay, and S. Merkel, Characterizing non-Markovian Off-Resonant Errors in Quantum Gates, [arXiv:2302.10881](https://arxiv.org/abs/2302.10881).
- [78] L. H. Pedersen, N. M. Møller, and K. Mølmer, Fidelity of quantum operations, *Phys. Lett. A* **367**, 47 (2007).
- [79] M. C. Collodo, J. Herrmann, N. Lacroix, C. K. Andersen, A. Remm, S. Lazar, J. Besse, T. Walter, A. Wallraff, and C. Eichler, Implementation of Conditional Phase Gates Based on Tunable ZZ Interactions, *Phys. Rev. Lett.* **125**, 240502 (2020).
- [80] Y. Xu, J. Chu, J. Yuan, J. Qiu, Y. Zhou, L. Zhang, X. Tan, Y. Yu, S. Liu, J. Li, F. Yan, and D. Yu, High-Fidelity, High-Scalability Two-Qubit Gate Scheme for Superconducting Qubits, *Phys. Rev. Lett.* **125**, 240503 (2020).
- [81] P. Zhao, K. Linghu, Z. Li, P. Xu, R. Wang, G. Xue, Y. Jin, and H. Yu, Quantum Crosstalk Analysis for Simultaneous Gate Operations on Superconducting Qubits, *PRX Quantum* **3**, 020301 (2022).
- [82] H. Goto, Double-Transmon Coupler: Fast Two-Qubit Gate with No Residual Coupling for Highly Detuned Superconducting Qubits, *Phys. Rev. Appl.* **18**, 034038 (2022).
- [83] D. L. Campbell, A.a Kamal, L. Ranzani, M. Senatore, and M. D. LaHaye, Modular Tunable Coupler for Superconducting Circuits, *Phys. Rev. Appl.* **19**, 064043 (2023).
- [84] R. Barends, J. Kelly, A. Megrant, A. Veitia, D. Sank, E. Jeffrey, T. C. White, J. Mutus, A. G. Fowler, B. Campbell *et al.*, Superconducting quantum circuits at the surface code threshold for fault tolerance, *Nature* **508**, 500 (2014).
- [85] S. Gustavsson, O. Zwiernik, J. Bylander, F. Yan, F. Yoshihara, Y. Nakamura, T. P. Orlando, and W. D. Oliver, Improving Quantum Gate Fidelities by Using a Qubit to Measure Microwave

- Pulse Distortions, *Phys. Rev. Lett.* **110**, 040502 (2013)
- [86] C. Müller, J. H. Cole, and J. Lisenfeld, Towards understanding two-level-systems in amorphous solids: insights from quantum circuits, *Rep. Prog. Phys.* **82**, 124501 (2019).
- [87] D. Dong and I. R. Petersen, Quantum control theory and applications: a survey, *IET Control. Theory Appl.* **4**, 2651 (2010).
- [88] J. B. Hertzberg, E. J. Zhang, S. Rosenblatt, E. Magesan, J. A. Smolin, J.-B. Yau, V. P. Adiga, M. Sandberg, M. Brink, Je. M. Chow, and J. S. Orcutt, Laser-annealing Josephson junctions for yielding scaled-up superconducting quantum processors, *npj Quantum Inf.* **7**, 129 (2021).
- [89] D. P. Pappas, M. Field, C. Kopas, J. A. Howard, X. Wang, E. Lachman, L. Zhou, J. Oh, K. Yadavalli, E. A. Sete, A. Bestwick, M. J. Kramer, and J. Y. Mutus, Alternating Bias Assisted Annealing of Amorphous Oxide Tunnel Junctions, [arXiv:2401.07415](https://arxiv.org/abs/2401.07415).
- [90] Y.-J. Hai, J. Li, J. Zeng, and X.-H. Deng, Universal robust quantum gates by geometric correspondence of noisy quantum dynamics, [arXiv:2210.14521](https://arxiv.org/abs/2210.14521).
- [91] B. Shao, X. Yang, R. Liu, Y. Zhai, D. Lu, T. Xin, and J. Li, Multiple Classical Noise Mitigation by Multiobjective Robust Quantum Optimal Control, [arXiv:2403.00298](https://arxiv.org/abs/2403.00298).
- [92] J. Kelly, P. O'Malley, M. Neeley, H. Neven, and J. M. Martinis, Physical qubit calibration on a directed acyclic graph, [arXiv:1803.03226](https://arxiv.org/abs/1803.03226).
- [93] P. V. Klimov, J. Kelly, J. M. Martinis, and H. Neven, The snake optimizer for learning quantum processor control parameters, [arXiv:2006.04594](https://arxiv.org/abs/2006.04594).
- [94] J. Kelly, R. Barends, A. G. Fowler, A. Megrant, E. Jeffrey, T. C. White, D. Sank, J. Y. Mutus, B. Campbell, Yu Chen, Z. Chen, B. Chiaro, A. Dunsworth, E. Lucero, M. Neeley, C. Neill, P. J. J. O'Malley, C. Quintana, P. Roushan, A. Vainsencher, J. Wenner, and John M. Martinis, Scalable *in situ* qubit calibration during repetitive error detection, *Phys. Rev. A* **94**, 032321 (2016).